AFRL-VA-WP-TP-2006-325

A HYPERSONIC VEHICLE MODEL DEVELOPED WITH PISTON THEORY (PREPRINT)

Michael W. Oppenheimer and David B. Doman

JULY 2006

Approved for public release; distribution is unlimited.

STINFO COPY

AIR VEHICLES DIRECTORATE
AIR FORCE MATERIEL COMMAND
AIR FORCE RESEARCH LABORATORY
WRIGHT-PATTERSON AIR FORCE BASE, OH 45433-7542

NOTICE AND SIGNATURE PAGE

Using Government drawings, specifications, or other data included in this document for any purpose other than Government procurement does not in any way obligate the U.S. Government. The fact that the Government formulated or supplied the drawings, specifications, or other data does not license the holder or any other person or corporation; or convey any rights or permission to manufacture, use, or sell any patented invention that may relate to them.

This report was cleared for public release by the Air Force Research Laboratory Wright Site (AFRL/WS) Public Affairs Office and is available to the general public, including foreign nationals. Copies may be obtained from the Defense Technical Information Center (DTIC) (http://www.dtic.mil).

AFRL-VA-WP-TP-2006-325 HAS BEEN REVIEWED AND IS APPROVED FOR PUBLICATION IN ACCORDANCE WITH ASSIGNED DISTRIBUTION STATEMENT.

*//Signature//

Michael W. Oppenheimer
Electronics Engineer
Control Design and Analysis Branch
Air Force Research Laboratory
Air Vehicles Directorate

//Signature//

Deborah S. Grismer
Chief
Control Design and Analysis Branch
Air Force Research Laboratory
Air Vehicles Directorate

//Signature//

Jeffrey C. Tromp
Senior Technical Advisor
Control Sciences Division
Air Force Research Laboratory
Air Vehicles Directorate

This report is published in the interest of scientific and technical information exchange, and its publication does not constitute the Government's approval or disapproval of its ideas or findings.

*Disseminated copies will show "//Signature//" stamped or typed above the signature blocks.

REPORT DOCUMENTATION PAGE

Form Approved
OMB No. 0704-0188

1. REPORT DATE *(DD-MM-YY)*	2. REPORT TYPE	3. DATES COVERED *(From - To)*
July 2006	Conference Paper Preprint	07/20/2005– 07/13/2006

4. TITLE AND SUBTITLE
A HYPERSONIC VEHICLE MODEL DEVELOPED WITH PISTON THEORY (PREPRINT)

5a. CONTRACT NUMBER
In-house

5b. GRANT NUMBER

5c. PROGRAM ELEMENT NUMBER
N/A

6. AUTHOR(S)
Michael W. Oppenheimer and David B. Doman

5d. PROJECT NUMBER
A03D

5e. TASK NUMBER

5f. WORK UNIT NUMBER
0B

7. PERFORMING ORGANIZATION NAME(S) AND ADDRESS(ES)
Control Design and Analysis Branch (AFRL/VACA)
Control Sciences Division
Air Vehicles Directorate
Air Force Materiel Command, Air Force Research Laboratory
Wright-Patterson Air Force Base, OH 45433-7542

8. PERFORMING ORGANIZATION REPORT NUMBER
AFRL-VA-WP-TP-2006-325

9. SPONSORING/MONITORING AGENCY NAME(S) AND ADDRESS(ES)
Air Vehicles Directorate
Air Force Research Laboratory
Air Force Materiel Command
Wright-Patterson Air Force Base, OH 45433-7542

10. SPONSORING/MONITORING AGENCY ACRONYM(S)
AFRL/VACA

11. SPONSORING/MONITORING AGENCY REPORT NUMBER(S)
AFRL-VA-WP-TP-2006-325

12. DISTRIBUTION/AVAILABILITY STATEMENT
Approved for public release; distribution is unlimited.

13. SUPPLEMENTARY NOTES
Report contains color.

This work has been submitted to the 2006 AIAA Guidance, Navigation, and Control Conference proceedings. This is a work of the U.S. Government and is not subject to copyright protection in the United States.

PAO Case Number: AFRL/WS 06-1783 (cleared July 19, 2006).

14. ABSTRACT

For high Mach number flows, $M \geq 4$, piston theory has been used to calculate the pressures on the surfaces of a vehicle. In a two-dimensional flow, a perpendicular column of fluid stays intact as it passes over a solid surface. Thus, the pressure at the surface can be calculated assuming the surface were a piston moving into a column of fluid. In this work, first-order piston theory is used to calculate the forces, moments, and stability derivatives for longitudinal motion of a hypersonic vehicle. Piston theory predicts a relationship between the local pressure on a surface and the normal component of fluid velocity produced by the surface's motion. The advantage of piston theory over other techniques, such as Prandtl-Meyer flow or Newtonian impact theory, is that unsteady aerodynamic effects can be included in the model. The unsteady effects, considered in this work, include perturbations in the linear velocities and angular rate. This provides a more accurate model that agrees more closely with models derived using computational fluid dynamics or those derived by solving Euler equations. Additionally, piston theory yields an analytical model for the longitudinal motion of the vehicle, thus allowing design trade studies to be performed while still providing insight into the physics of the problem.

15. SUBJECT TERMS
Piston Theory, Hypersonic Vehicles, Unsteady Aerodynamics

16. SECURITY CLASSIFICATION OF:			17. LIMITATION OF ABSTRACT:	18. NUMBER OF PAGES	19a. NAME OF RESPONSIBLE PERSON (Monitor)
a. REPORT	b. ABSTRACT	c. THIS PAGE			Michael W. Oppenheimer
Unclassified	Unclassified	Unclassified	SAR	30	19b. TELEPHONE NUMBER *(Include Area Code)* N/A

A Hypersonic Vehicle Model Developed With Piston Theory

Michael W. Oppenheimer *
David B. Doman †
Air Force Research Laboratory, WPAFB, OH 45433-7531

I. Abstract

For high Mach number flows, $M \geq 4$, piston theory has been used to calculate the pressures on the surfaces of a vehicle. In a two-dimensional inviscid flow, a perpendicular column of fluid stays intact as it passes over a solid surface. Thus, the pressure at the surface can be calculated assuming the surface were a piston moving into a column of fluid. In this work, first-order piston theory is used to calculate the forces, moments, and stability derivatives for longitudinal motion of a hypersonic vehicle. Piston theory predicts a relationship between the local pressure on a surface and the normal component of fluid velocity produced by the surface's motion. The advantage of piston theory over other techniques, such as Prandtl-Meyer flow, oblique shock, or Newtonian impact theory, is that unsteady aerodynamic effects can be included in the model. The unsteady effects, considered in this work, include perturbations in the linear velocities and angular rates, due to rigid body motion. This provides a more accurate model that agrees more closely with models derived using computational fluid dynamics or those derived by solving Euler equations. Additionally, piston theory yields an analytical model for the longitudinal motion of the vehicle, thus allowing design trade studies to be performed while still providing insight into the physics of the problem.

II. Introduction

In the 1980's, the National Aerospace Plane (NASP) program commenced, with its goal being a feasibility study for a single-stage to orbit (SSTO) vehicle, which was reusable and could take off and land horizontally. The NASP was to be powered by a supersonic combustion ramjet (scramjet) engine. Although this program was cancelled in the 1990's, a great deal of knowledge was gained and it spawned future programs, including the hypersonic systems technology program (HySTP), initiated in late 1994, and the NASA X-43A. The HySTP program's goal was to transfer the accomplishments of the NASP program to a technology demonstration program. This program was cancelled in early 1995. The NASA X-43A set new world speed records in 2004, reaching Mach 6.8 and Mach 9.6 on two separate occasions with a scramjet engine. These flights were the culmination of NASA's Hyper-X program, with the objective being to explore alternatives to rocket power for space access vehicles.

With renewed interest in space operations worldwide, there is a renewed interest in hypersonic aerodynamics research. The scramjet engine will likely play a major role in future hypersonic vehicles. Ulinke a conventional turbojet engine, a scramjet engine does not use high speed turbomachinery to compress the air before it reaches the combustor. Instead, it relies upon the rise in pressure across oblique shock waves located in front of the inlet. Furthermore, the flow through the entire engine is supersonic in contract to a ramjet where the flow speeds are subsonic through the combustor. On configurations like the NASP and X-43A,

*Electronics Engineer, Control Theory and Optimization Branch, 2210 Eighth Street, Ste 21, Email Michael.Oppenheimer@wpafb.af.mil, Ph. (937) 255-8490, Fax (937) 656-4000, Member AIAA
†Senior Aerospace Engineer, Control Theory and Optimization Branch, 2210 Eighth Street, Ste 21, Email David.Doman@wpafb.af.mil, Ph. (937) 255-8451, Fax (937) 656-4000, Senior Member AIAA

the underside of the airframe must function as the air inlet mechanism and the exhaust nozzle. Therefore, integration of the airframe and engine are critical to success of a scramjet powered vehicle.

Scramjets could be used as part of a multi-stage launch vehicle that would include multiple propulsion systems to perform a mission. The factor driving research towards scramjets and away from rockets is cost; scramjets would substantially lower costs because it is an airbreathing engine. Airbreathing engines don't require oxidizer to be carried by the vehicle, hence increasing the payload and reducing the quantity of fuel carried.

Unsteady aerodynamics is another key technology in the development and optimization of future hypersonic vehicles. The combined effects of a slender flexible vehicle travelling at high speeds and subjected to large forces may lead to significant unsteady aerodynamic effects. Hence, understanding the concepts and consequences of time-dependent aerodynamic flows is critical to the success of this type of vehicle.

Piston theory is a technique which has been used for years to determine the pressure distributions on an airfoil/vehicle, when the Mach number is sufficiently high. Lighthill[1] discussed the application of piston theory on oscillating airfoils some 50 years ago. Ashley and Zartarian[2] discuss piston theory while providing a number of examples of the application of piston theory to specific problems. More recently, Tarpley[3] discussed the computation of stability derivatives for a caret-wing waverider using piston theory. Estimation of stability derivatives also requires the analysis of unsteady flow over the vehicle.[3] Piston theory allows the inclusion of unsteady aerodynamic effects in the model and a closed form solution can be found for these unsteady effects.

In this work, piston theory is applied to a hypothetical 2-dimensional hypersonic vehicle powered with a scramjet. Section III describes the vehicle analyzed in this work, while the steady forces on the vehicle's surfaces are calculated in Section IV. The afterbody effects are included in Section V, where the pressure distribution and force due to exhaust plume are evaluated. The control surface, which is a single elevator, is examined in Section VI, analysis of the flow regions is performed in Section VII, total body forces and moments are derived in Section VIII, while stability derivatives are calculated in Section IX. The engine model is developed in Section X and some results from an open-loop simulation are provided in Section XI.

III. HSV Model

Figure 1 shows the hypersonic vehicle considered in this work.[4] The vehicle consists of 4 surfaces: an upper surface (surfaces defined by points cf) and three lower surfaces (surfaces defined by points cd, gh, and ef). All pertinent lengths and dimensions are in units of feet and degrees, respectively. The total length of the vehicle is $L = 100ft$ and the notation for lengths is L_f = length of the forebody, L_e = length of the engine nacelle, L_a = length of the aftbody, L_e is the length of the elevator, $\bar{x}_f$ is the distance from the C.G. to the front of the vehicle, $\bar{x}_a$ is the distance from the C.G. to the rear of the vehicle, x_{cs} and z_{cs} are the distances from the C.G. to the midpoint of the elevator in the x and z directions, respectively, and h_i is the engine height. The vehicle lengths are

$$\begin{aligned} L &= 100\ ft \\ L_f &= 47\ ft \\ L_a &= 33\ ft \\ L_n &= 20\ ft \\ L_e &= 17\ ft \\ \bar{x}_f &= 55\ ft \\ \bar{x}_a &= 45\ ft \\ x_{cs} &= 30\ ft \\ z_{cs} &= 3.5\ ft \\ h_i &= 3.5\ ft \end{aligned} \tag{1}$$

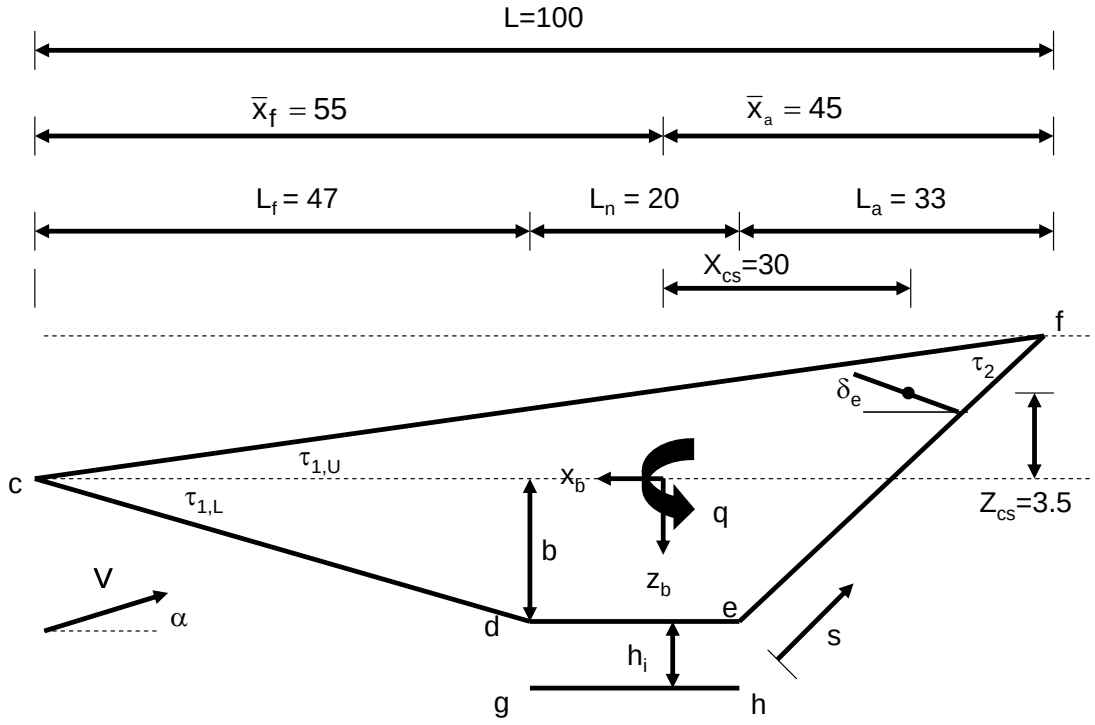

Figure 1. Hypersonic Vehicle.

The vehicle angles are

$$\begin{aligned} \tau_{1,U} &= 3^\circ \\ \tau_{1,L} &= 6^\circ \\ \tau_2 &= 14.41^\circ \end{aligned} \tag{2}$$

Additionally, the vehicle mass and moment of inertia are

$$\begin{aligned} Mass &= 300\ slug \\ J_{yy} &= 500,000\ slug - ft^2 \end{aligned} \tag{3}$$

and the mean aerodynamic chord ($\bar{c}$) and planform area (S) are defined as

$$\begin{aligned} \bar{c} &= L \\ S &= L^2 \end{aligned} \tag{4}$$

The goal is to apply piston theory to this vehicle to determine the pressure distribution on the surfaces of the vehicle, which, in turn, can be used to evaluate the forces and moments. The pressure on the face of a piston moving into a column of perfect gas is[2]

$$\frac{P}{P_\infty} = \left(1 + \frac{\gamma - 1}{2}\frac{V_n}{a_\infty}\right)^{\frac{2\gamma}{\gamma-1}} \tag{5}$$

where the subscript "∞" refers to the steady flow conditions past the surface, V_n is the velocity of the surface normal to the steady flow, a_∞ is the freestream speed of sound, and P is the surface pressure. Taking the binomial expansion of Eq. 5 produces

$$\frac{P}{P_\infty} = 1 + \frac{2\gamma}{\gamma - 1}\frac{\gamma - 1}{2}\frac{V_n}{a_\infty} = 1 + \frac{\gamma V_n}{a_\infty} \tag{6}$$

Multiplying through by P_∞ and using the perfect gas law ($P = \rho RT$) and the definition of the speed of sound ($a^2 = \gamma RT$) yields the basic result from first-order linear piston theory

$$P = P_\infty + \rho_\infty a_\infty V_n \tag{7}$$

The infinitesimal force due to the pressure is

$$d\mathbf{F} = -P dA \mathbf{n} \tag{8}$$

where dA is a surface element and $\mathbf{n}$ is the outward pointing normal. Substituting Eq. 7 into Eq. 8 yields

$$d\mathbf{F} = \left(-P_\infty - \rho_\infty a_\infty V_n\right) dA \mathbf{n} \tag{9}$$

The normal velocity can be computed by taking the dot product of the flow velocity over a surface and the outward pointing normal for that surface. Hence, Eq. 9 becomes

$$d\mathbf{F} = \left(-P_\infty - \rho_\infty a_\infty \left[\mathbf{V} \cdot \mathbf{n}\right]\right) dA \mathbf{n} \tag{10}$$

Equation 10 is the basic result upon which this work is based. From this equation, it is seen that in order to compute the forces acting on a surface, one must determine the properties of the flow past the surface (properties behind a shock, expansion fan, or freestream), the velocity of the surface relative to the airstream, $\mathbf{V}$, the outward pointing surface normal, $\mathbf{n}$, and the surface element, dA. The work that follows will develop these necessary quantities for the upper surface and the lower surfaces defined by points (cd) and (gh).

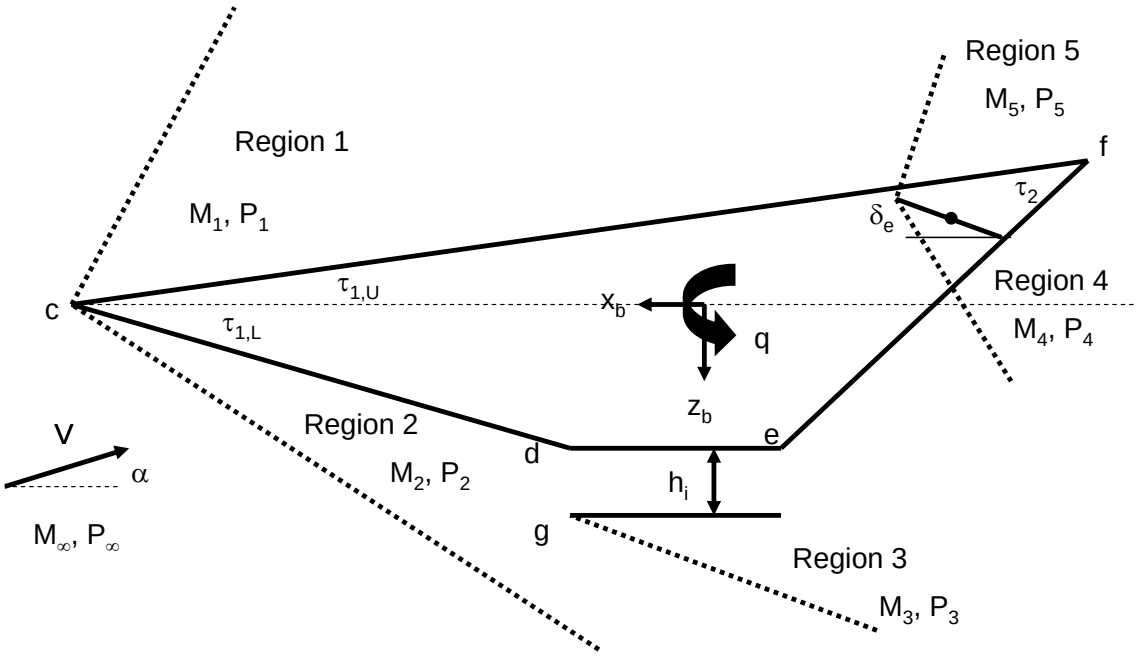

Figure 2. Hypersonic Vehicle, Oblique Shocks, and Pressure Regions.

IV. Vehicle Surface Pressure Distributions and Forces

To compute the forces, moments, and stability derivatives, consider small perturbations, from a steady flight condition at M_∞, in the velocities u and w and the rate q. On the upper surface, the surface is modelled as a piston moving into a column of fluid that has the properties of the flow behind an oblique shock wave (an oblique shock forms if $\alpha < \tau_{1,U}$). Likewise, on the lower surface, the surface is modelled as a piston moving into a column of fluid that has the properties of the fluid behind the oblique shock. Figure 2 shows the regions of interest.

To begin the development, first consider the upper surface. The velocity of a point on the upper surface due to the velocity and rate perturbations is

$$\mathbf{V}_{cf} = (V_1 \cos\tau_{1,U} + u)\,\hat{i} + (V_1 \sin\tau_{1,U} + w)\,\hat{k} + \boldsymbol{\omega} \times \mathbf{r}_{cf} \tag{11}$$

where $\hat{i}, \hat{k}$ are unit vectors in the x and z body axes, respectively, $\boldsymbol{\omega}$ is the angular rate vector, α is the angle of attack, and V_1 is the velocity of the flow behind the oblique shock wave (see region 1 in Fig. 2). For longitudinal motion only, $\boldsymbol{\omega} = q\hat{j}$ where $\hat{j}$ is a unit vector in the y body axis direction. In Eq. 11, $\mathbf{r}_u$ is the position vector of a point on the upper surface given by

$$\begin{gathered}\mathbf{r}_{cf} = r_{cf_x}\hat{i} + + r_{cf_z}\hat{k} = x\hat{i} + \tan\tau_{1,U}\,(x - \bar{x}_f)\,\hat{k} \\ -\bar{x}_a \le x \le \bar{x}_f\end{gathered} \tag{12}$$

According to Eq. 8, a normal vector to the upper surface is also needed. The upper surface outward pointing normal vector is

$$\mathbf{n}_{cf} = \sin\tau_{1,U}\hat{i} - \cos\tau_{1,U}\hat{k} \tag{13}$$

For the lower surface defined by the points c and d in Figure 1, we use the velocity of the flow after the oblique shock to obtain

$$\mathbf{V}_{cd} = (V_2 \cos\tau_{1,L} + u)\,\hat{i} + (-V_2 \sin\tau_{1,L} + w)\,\hat{k} + \boldsymbol{\omega} \times \mathbf{r}_{cd} \tag{14}$$

while for the surface defined by points g and h

$$\mathbf{V}_{gh} = (V_3 + u)\,\hat{i} + w\hat{k} + \boldsymbol{\omega} \times \mathbf{r}_{gh} \tag{15}$$

where $\mathbf{r}_{cd}$ and $\mathbf{r}_{gh}$ are position vectors of a point on the lower surface given by

$$\begin{gathered} \mathbf{r}_{cd} = r_{cd_x}\hat{i} + r_{cd_z}\hat{k} = x\hat{i} - \tan\tau_{1,L}\,(x - \bar{x}_f)\,\hat{k} \\ \bar{x}_f - L_f \leq x \leq \bar{x}_f \end{gathered} \tag{16}$$

$$\begin{gathered} \mathbf{r}_{gh} = r_{gh_x}\hat{i} + r_{gh_z}\hat{k} = x\hat{i} + (L_f \tan\tau_{1,L} + h_i)\,\hat{k} \\ (\bar{x}_f - L_f) - L_n \leq x \leq \bar{x}_f - L_f \end{gathered} \tag{17}$$

The normal vectors for the lower surfaces are

$$\begin{gathered} \mathbf{n}_{cd} = \sin\tau_{1,L}\hat{i} + \cos\tau_{1,L}\hat{k} \\ \mathbf{n}_{gh} = 1\hat{k} \end{gathered} \tag{18}$$

Performing the cross products required by Eqs. 11, 14, and 15 gives

$$\boldsymbol{\omega} \times \mathbf{r}_{cf} = q\tan\tau_{1,U}\,(x - \bar{x}_f)\,\hat{i} - qx\hat{k} \tag{19}$$

$$\boldsymbol{\omega} \times \mathbf{r}_{cd} = -q\tan\tau_{1,L}\,(x - \bar{x}_f)\,\hat{i} - qx\hat{k} \tag{20}$$

$$\boldsymbol{\omega} \times \mathbf{r}_{gh} = q\,(L_f\tan\tau_{1,L} + h_i)\,\hat{i} - qx\hat{k} \tag{21}$$

According to Eq. 10, the pressures on the surfaces of interest are

$$\begin{aligned} P_{cf} &= P_1 + \rho_1 a_1\,(\mathbf{V}_{cf} \cdot \mathbf{n}_{cf}) \\ P_{cd} &= P_2 + \rho_2 a_2\,(\mathbf{V}_{cd} \cdot \mathbf{n}_{cd}) \\ P_{gh} &= P_3 + \rho_3 a_3\,(\mathbf{V}_{gh} \cdot \mathbf{n}_{gh}) \end{aligned} \tag{22}$$

Substituting the results of Eq. 22 into Eq. 8 gives

$$\begin{aligned} d\mathbf{F}_{cf} &= \{-P_1 - \rho_1 a_1\,(\mathbf{V}_{cf} \cdot \mathbf{n}_{cf})\}\,dA_{cf}\mathbf{n}_{cf} \\ d\mathbf{F}_{cd} &= \{-P_2 - \rho_2 a_2\,(\mathbf{V}_{cd} \cdot \mathbf{n}_{cd})\}\,dA_{cd}\mathbf{n}_{cd} \\ d\mathbf{F}_{gh} &= \{-P_3 - \rho_3 a_3\,(\mathbf{V}_{gh} \cdot \mathbf{n}_{gh})\}\,dA_{gh}\mathbf{n}_{gh} \end{aligned} \tag{23}$$

Using Eqs. 11, 14, and 15 and the appropriate normal vectors (Eqs. 13 and 18), the dot products in Eq. 23 become

$$\begin{aligned} \mathbf{V}_{cf} \cdot \mathbf{n}_{cf} &= [u + q\tan\tau_{1,U}\,(x - \bar{x}_f)]\sin\tau_{1,U} - [w - qx]\cos\tau_{1,U} \\ \mathbf{V}_{cd} \cdot \mathbf{n}_{cd} &= [u - q\tan\tau_{1,L}\,(x - \bar{x}_f)]\sin\tau_{1,L} + [w - qx]\cos\tau_{1,L} \\ \mathbf{V}_{gh} \cdot \mathbf{n}_{gh} &= w - qx \end{aligned} \tag{24}$$

Note that the steady terms cancel as a result of taking the dot product. Using Eq. 24 in Eq. 23 yields

$$\begin{aligned} d\mathbf{F}_{cf} &= (-P_1 - \rho_1 a_1\,\{[u + q\tan\tau_{1,U}\,(x - \bar{x}_f)]\sin\tau_{1,U} - [w - qx]\cos\tau_{1,U}\})\,dA_{cf}\mathbf{n}_{cf} \\ d\mathbf{F}_{cd} &= (-P_2 - \rho_2 a_2\,\{[u - q\tan\tau_{1,L}\,(x - \bar{x}_f)]\sin\tau_{1,L} + [w - qx]\cos\tau_{1,L}\})\,dA_{cd}\mathbf{n}_{cd} \\ d\mathbf{F}_{gh} &= (-P_3 - \rho_3 a_3\,\{w - qx\})\,dA_{gh}\mathbf{n}_{gh} \end{aligned} \tag{25}$$

The next step is to determine the upper and lower surface elements. Note that the vehicle model is 2-dimensional with unit depth into the page. Hence, the upper surface element, dA_u can be written as

$$dA_{cf} = dL_{cf}(1) \tag{26}$$

where dL_{cf} defines a length of interest on the upper surface and the multiplying factor of 1 is due to the vehicle's unit depth. The surface element can be written as

$$dA_{cf} = \sqrt{dx^2 + dz^2}(1) \tag{27}$$

From Eq. 12,

$$z = \tan\tau_{1,U}\left(x - \bar{x}_f\right) \Rightarrow dz = \tan\tau_{1,U}dx \tag{28}$$

Using Eq. 28 in Eq. 27 yields

$$dA_{cf} = \sqrt{dx^2 + \tan^2\tau_{1,U}dx^2}(1) = dx\sqrt{1 + \tan^2\tau_{1,U}}(1) = dx\sec\tau_{1,U}(1) = \sec\tau_{1,U}dx \tag{29}$$

Similarly, the surface elements for the lower surfaces become

$$dA_{cd} = \sec\tau_{1,L}dx \tag{30}$$

$$dA_{gh} = dx \tag{31}$$

Now, the incremental force on the upper surface (see first entry in Eq. 25) becomes

$$d\mathbf{F}_{cf} = \left(-P_1 - \rho_1 a_1\left\{\left[u + q\tan\tau_{1,U}\left(x - \bar{x}_f\right)\right]\sin\tau_{1,U} - \left[w - qx\right]\cos\tau_{1,U}\right\}\right)\mathbf{n}_{cf}\sec\tau_{1,U}dx \tag{32}$$

Using similar analysis, the incremental forces on the lower surfaces become

$$d\mathbf{F}_{cd} = \left(-P_2 - \rho_2 a_2\left\{\left[u - q\tan\tau_{1,L}\left(x - \bar{x}_f\right)\right]\sin\tau_{1,L} + \left[w - qx\right]\cos\tau_{1,L}\right\}\right)\mathbf{n}_{cd}\sec\tau_{1,L}dx \tag{33}$$

$$d\mathbf{F}_{gh} = \left(-P_3 - \rho_3 a_3\left\{w - qx\right\}\right)\mathbf{n}_{gh}dx \tag{34}$$

It will be useful to separate the steady forces from the unsteady forces at this point. In Section IX, we will model the unsteady effects using a stability derivative approach. To compute the steady forces, the components of the incremental forces related to the steady flow are integrated over the surface of the vehicle. For the upper surface, this becomes

$$\mathbf{F}_{cf} = \int_{-\bar{x}_a}^{\bar{x}_f}\left(d\mathbf{F}_{cf}\right)_{steady} = \int_{-\bar{x}_a}^{\bar{x}_f} -P_1\left[\sin\tau_{1,U}\hat{i} - \cos\tau_{1,U}\hat{k}\right]\sec\tau_{1,U}dx \tag{35}$$

while, for the lower surfaces, the forces are

$$\mathbf{F}_{cd} = \int_{\bar{x}_f - L_f}^{\bar{x}_f}\left(d\mathbf{F}_{cd}\right)_{steady} = \int_{\bar{x}_f - L_f}^{\bar{x}_f} -P_2\left[\sin\tau_{1,L}\hat{i} + \cos\tau_{1,L}\hat{k}\right]\sec\tau_{1,L}dx \tag{36}$$

$$\mathbf{F}_{gh} = \int_{(\bar{x}_f - L_f) - L_n}^{\bar{x}_f - L_f}\left(d\mathbf{F}_{gh}\right)_{steady} = \int_{(\bar{x}_f - L_f) - L_n}^{\bar{x}_f - L_f} -P_3\hat{k}dx \tag{37}$$

For the consideration of aeroelastic effects in future work, it will prove useful to split the upper surface force into forebody and afterbody components. Thus, Eq. 35 becomes

$$\begin{aligned}\mathbf{F}_{cf} &= \int_{-\bar{x}_a}^{0} -P_1\left[\sin\tau_{1,U}\hat{i} - \cos\tau_{1,U}\hat{k}\right]\sec\tau_{1,U}dx + \int_{0}^{\bar{x}_f} -P_1\left[\sin\tau_{1,U}\hat{i} - \cos\tau_{1,U}\hat{k}\right]\sec\tau_{1,U}dx \\ &= \mathbf{F}_{cf_a} + \mathbf{F}_{cf_f}\end{aligned} \tag{38}$$

Performing the integrations yields

$$\begin{aligned}\mathbf{F}_{cf_a} &= -P_1\bar{x}_a\sec\tau_{1,U}\left[\sin\tau_{1,U}\hat{i} - \cos\tau_{1,U}\hat{k}\right] = X_{cf_a}\hat{i} + Z_{cf_a}\hat{k} \\ \mathbf{F}_{cf_f} &= -P_1\bar{x}_f\sec\tau_{1,U}\left[\sin\tau_{1,U}\hat{i} - \cos\tau_{1,U}\hat{k}\right] = X_{cf_f}\hat{i} + Z_{cf_f}\hat{k}\end{aligned} \tag{39}$$

where X_{cf_a}, Z_{cf_a} are the components of the aftbody upper surface force in the x and z directions, respectively, and X_{cf_f}, Z_{cf_f} are the components of the forebody upper surface force in the x and z directions. For the lower surfaces, integration of Eqs. 36 and 37 produce

$$\begin{aligned}\mathbf{F}_{cd} &= -P_2 L_f\sec\tau_{1,L}\left[\sin\tau_{1,L}\hat{i} + \cos\tau_{1,L}\hat{k}\right] = X_{cd}\hat{i} + Z_{cd}\hat{k} \\ \mathbf{F}_{gh} &= -P_3 L_n\hat{k} = X_{gh}\hat{i} + Z_{gh}\hat{k}\end{aligned} \tag{40}$$

where X_* and Z_* are the components of the lower surface forces. Equations 39 and 40 give the rigid body steady forces on this vehicle due to pressure distributions on the upper and lower surfaces (cd and gh). It must still be determined where these forces act on the surfaces. To do this, note that the steady pressures on the surfaces are simply the pressure behind the shock wave or expansion fan or the freestream pressure, depending on the angle of attack of the vehicle.

V. Afterbody

The flow on the afterbody of the vehicle is bounded by the vehicle surface (surface ef in Fig. 1) and a shear layer between the freestream atmosphere and the exhaust gas of the engine. Hence, external nozzle analysis must be performed to determine the pressures on surface ef. According to Chavez,[5] the pressure distribution along the nozzle surface can be approximated by

$$P_{ef}(s) \approx \frac{P_e}{1 + \frac{s}{\frac{L_a}{\cos(\tau_{1,U}+\tau_2)}}\left(\frac{P_e}{P_\infty} - 1\right)} \tag{41}$$

where P_{ef} is the pressure on the afterbody, P_e is the pressure at the engine exit, P_∞ is the freestream pressure, and s is the distance from the lower apex (point e) to the point of interest along the vehicle's afterbody surface (see Fig. 1). The force produced by the external nozzle can be calculated by integrating Eq. 41 over the rear ramp of the vehicle:

$$F_{ef} = \int_0^{\frac{L_a}{\cos(\tau_{1,U}+\tau_2)}} \frac{P_e}{1 + \frac{s}{\frac{L_a}{\cos(\tau_{1,U}+\tau_2)}}\left(\frac{P_e}{P_\infty} - 1\right)} ds \tag{42}$$

Performing the integration and simplifying yields

$$F_{ef} = \frac{L_a P_e P_\infty}{\cos(\tau_{1,U}+\tau_2)(P_e - P_\infty)} \ln\frac{P_e}{P_\infty} \tag{43}$$

Equation 43 provides the magnitude of the force due to the external nozzle. Its direction is perpendicular to the rear ramp. Hence, the vector force due to the external nozzle is

$$\mathbf{F}_{ef} = \frac{L_a P_e P_\infty}{\cos(\tau_{1,U}+\tau_2)(P_e - P_\infty)} \ln\frac{P_e}{P_\infty}\left[\sin(\tau_{1,U}+\tau_2)\,\hat{i} - \cos(\tau_{1,U}+\tau_2)\,\hat{k}\right] = X_{ef}\hat{i} + Z_{ef}\hat{k} \tag{44}$$

where X_{ef} and Z_{ef} are the axial and normal force components of the external nozzle force.

For use in calculating stability derivatives, it is necessary to determine the force on the rear ramp due to perturbations in the velocities u and w and the rate q. The differential force on the rear ramp is

$$d\mathbf{F}_{ef} = \left(-P_{ef} - \rho_{ef} a_{ef}\left[\mathbf{V}_{ef}\cdot\mathbf{n}_{ef}\right]\right) dA_{ef}\mathbf{n}_{ef} \tag{45}$$

where P_{ef} is the afterbody pressure distribution given by Eq. 41, ρ_{ef}, a_{ef} are the density and speed of sound on the rear ramp, $\mathbf{V}_{ef}$ is the flow velocity on lower surface ef, $\mathbf{n}_{ef}$ is the normal vector to lower surface ef, and dA_{ef} is the surface element for surface ef. The position vector, normal vector, and surface element for this surface are given by:

$$\begin{gathered}\mathbf{r}_{ef} = x\hat{i} + \left[\tan(\tau_{1,U}+\tau_2)(x+\bar{x}_a) - L\tan\tau_{1,U}\right]\hat{k} = x\hat{i} + r_{ef_z}\hat{k} \\ -\bar{x}_a \le x \le L_a - \bar{x}_a\end{gathered} \tag{46}$$

$$\mathbf{n}_{ef} = -\sin(\tau_{1,U}+\tau_2)\,\hat{i} + \cos(\tau_{1,U}+\tau_2)\,\hat{k} \tag{47}$$

$$dA_{ef} = \sec(\tau_{1,U}+\tau_2)\,dx \tag{48}$$

Using Eqs. 46- 48 in Eq. 45 yields

$$d\mathbf{F}_{ef} = \left(-P_{ef} - \rho_{ef}a_{ef}\left\{-(u+qr_{ef_z})\sin(\tau_{1,U}+\tau_2) + (w-qx)\cos(\tau_{1,U}+\tau_2)\right\}\right)\mathbf{n}_{ef}dA_{ef} \tag{49}$$

Integration of the steady component of Eq. 49 yields the same result as in Eq. 44. The unsteady components will be utilized in the computation of stability derivatives.

VI. Control Surfaces

The control surface is an elevator located near the tail of the vehicle as shown in Fig. 1. The elevator is modelled as a flat plate hinged at its midpoint so the entire surface deflects. The length of the elevator is $L_e = 17ft$. Positive δ_e is defined as trailing edge down. Once again, the velocity of the flow on both sides of the elevator must be determined. Proceeding in a manner similar to that which has already been done, it is found that

$$\mathbf{V}_{e_L} = (V_4 \cos\delta_e + u)\,\hat{i} + (-V_4 \sin\delta_e + w)\,\hat{k} + \boldsymbol{\omega} \times \mathbf{r}_e \tag{50}$$

and

$$\mathbf{V}_{e_U} = (V_5 \cos\delta_e + u)\,\hat{i} + (-V_5 \sin\delta_e + w)\,\hat{k} + \boldsymbol{\omega} \times \mathbf{r}_e \tag{51}$$

where V_{e_L} is the flow velocity on the underside of the elevator, V_{e_U} is the flow velocity on the upper surface of the elevator, $\boldsymbol{\omega} = q\hat{j}$, $\mathbf{r}_e$ is a position vector from the vehicle c.g. to an arbitrary point on the elevator, V_4, V_5 are fluid velocities (freestream, behind oblique shock, or behind expansion fan).

The position vector is found to be

$$\begin{gathered} \mathbf{r}_e = x\hat{i} - [z_{cs} + \tan\delta_e\,(x + x_{cs})]\,\hat{k} \\ -x_{cs} - \tfrac{L_e}{2}\cos\delta_e \le x \le -x_{cs} + \tfrac{L_e}{2}\cos\delta_e \end{gathered} \tag{52}$$

where x_{cs} and z_{cs} are the x and z positions of the midpoint of the elevator referenced to the c.g. As shown in Fig. 1, $x_{cs} = -30ft$ and $z_{cs} = -3.5ft$. For this control surface, outward pointing normal vectors for both the lower and upper surfaces are needed. These normals are computed as

$$\begin{aligned} \mathbf{n}_{e_U} &= -\sin\delta_e\hat{i} - \cos\delta_e\hat{k} \\ \mathbf{n}_{e_L} &= \sin\delta_e\hat{i} + \cos\delta_e\hat{k} \end{aligned} \tag{53}$$

To evaluate the cross-product in Eq. 51, we use Eq. 52 to obtain

$$\boldsymbol{\omega} \times \mathbf{r}_e = -q\,[z_{cs} + \tan\delta_e\,(x - x_{cs})]\,\hat{i} - qx\hat{k} \tag{54}$$

Then, the differential forces on the upper and lower surfaces of the elevator becomes

$$\begin{aligned} d\mathbf{F}_{e_U} &= [-P_5 - \rho_5 a_5\,\{\mathbf{V}_{e_U} \cdot \mathbf{n}_{e_U}\}]\,\mathbf{n}_{e_U}\,dA_e \\ d\mathbf{F}_{e_L} &= [-P_4 - \rho_4 a_4\,\{\mathbf{V}_{e_L} \cdot \mathbf{n}_{e_L}\}]\,\mathbf{n}_{e_L}\,dA_e \end{aligned} \tag{55}$$

where

$$\mathbf{V}_{e_U} \cdot \mathbf{n}_{e_U} = -\left(u - q\,\{z_{cs} + \tan\delta_e\,(x - x_{cs})\}\right)\sin\delta_e - (w - qx)\cos\delta_e \tag{56}$$

$$\mathbf{V}_{e_L} \cdot \mathbf{n}_{e_L} = \left(u - q\,\{z_{cs} + \tan\delta_e\,(x - x_{cs})\}\right)\sin\delta_e + (w - qx)\cos\delta_e \tag{57}$$

and

$$dA_e = \sec\delta_e dx(1) = \sec\delta_e dx \tag{58}$$

Hence, the upper and lower forces on the elevator can be computed as

$$\mathbf{F}_{e_U} = \int_{-x_{cs}-\frac{L_e}{2}\cos\delta_e}^{-x_{cs}+\frac{L_e}{2}\cos\delta_e} [-P_5 - \rho_5 a_5\,\{\mathbf{V}_{e_U} \cdot \mathbf{n}_{e_U}\}]\left[-\sin\delta_e\hat{i} - \cos\delta_e\hat{k}\right]\sec\delta_e dx \tag{59}$$

$$\mathbf{F}_{e_L} = \int_{-x_{cs}-\frac{L_e}{2}\cos\delta_e}^{-x_{cs}+\frac{L_e}{2}\cos\delta_e} [-P_4 - \rho_4 a_4\,\{\mathbf{V}_{e_L} \cdot \mathbf{n}_{e_L}\}]\left[\sin\delta_e\hat{i} + \cos\delta_e\hat{k}\right]\sec\delta_e dx \tag{60}$$

Eq. 56 would be used in Eq. 59, while Eq. 57 would be used in Eq. 60. The steady forces on the elevator become

$$\mathbf{F}_{e_U} = \int_{-x_{cs}-\frac{L_e}{2}\cos\delta_e}^{-x_{cs}+\frac{L_e}{2}\cos\delta_e} -P_5\left[-\sin\delta_e\hat{i} - \cos\delta_e\hat{k}\right]\sec\delta_e dx \tag{61}$$

$$\mathbf{F}_{e_L} = \int_{-x_{cs}-\frac{L_e}{2}\cos\delta_e}^{-x_{cs}+\frac{L_e}{2}\cos\delta_e} -P_4\left[\sin\delta_e\hat{i} + \cos\delta_e\hat{k}\right]\sec\delta_e dx \tag{62}$$

Evaluating these integrals yields

$$\mathbf{F}_{e_U} = -P_5 L_e\left[-\sin\delta_e\hat{i} - \cos\delta_e\hat{k}\right] = X_{e_U}\hat{i} + Z_{e_U}\hat{k} \tag{63}$$

$$\mathbf{F}_{e_L} = -P_4 L_e\left[\sin\delta_e\hat{i} + \cos\delta_e\hat{k}\right] = X_{e_L}\hat{i} + Z_{e_L}\hat{k} \tag{64}$$

VII. Flow Analysis

In the preceding analysis, the properties of the flow on the upper, lower, and control surfaces has been left general. In this section, the properties of the flow will be determined. Specifically, the angles of attack at which shock waves or expansion fans are created will be delineated.

By examination of Fig. 1, the following relationships can be determined:

$$\begin{gathered} if\ \ \alpha = \tau_{1,U} \rightarrow freestream : V_1 = V_\infty, \rho_1 = \rho_\infty, a_1 = a_\infty \\ if\ \ \alpha > \tau_{1,U} \rightarrow expansionfan \\ if\ \ \alpha < \tau_{1,U} \rightarrow shock(compression) \end{gathered} \tag{65}$$

The wedge angles associated with the upper surface, for calculation of flow properties behind the shock or expansion fan, are as follows:

$$\begin{gathered} if\ \ \alpha > \tau_{1,U} \rightarrow \theta_{U_{expansion}} = \alpha - \tau_{1,U} \\ if\ \ \alpha < \tau_{1,U} \rightarrow \theta_{U_{shock}} = -\alpha + \tau_{1,U} \end{gathered} \tag{66}$$

The above information is used to determine the flow properties for the upper surface, namely, V_1, ρ_1, and a_1. For lower surface cd, the relationships become

$$\begin{gathered} if\ \ \alpha = -\tau_{1,L} \rightarrow freestream : V_2 = V_\infty, \rho_2 = \rho_\infty, a_2 = a_\infty \\ if\ \ \alpha > -\tau_{1,L} \rightarrow shock(compression) \\ if\ \ \alpha < -\tau_{1,L} \rightarrow expansionfan \end{gathered} \tag{67}$$

Lower surface cd wedge angles are as follows:

$$\begin{gathered} if\ \ \alpha > -\tau_{1,L} \rightarrow \theta_{L_{shock}} = \alpha + \tau_{1,L} \\ if\ \ \alpha < -\tau_{1,L} \rightarrow \theta_{L_{expansion}} = -\alpha - \tau_{1,L} \end{gathered} \tag{68}$$

Physically, for the scramjet engine to work properly, an oblique shock must form on the underside of the vehicle to increase the pressure at the inlet. This effectively places a lower limit on the angle of attack and requires that the angle of attack be such that an oblique shock forms on the underside of the vehicle. Hence, from Eq. 67, the angle of attack must satisfy

$$\alpha > -\tau_{1,L} \tag{69}$$

In other words, $-\tau_{1,L}$ is an absolute lower limit for angle of attack, with the engine on; however, the engine will cease to function before this lower limit is reached. With this limit in place, a bow shock will form on the underside of the vehicle. For lower surface gh, it is necessary to calculate the angle at which the shock exactly impinges on the point g of the engine nacelle. This angle, denoted by $\tau_{bowshock}$, is

$$\tau_{bowshock} = \alpha + \tan^{-1}\left(\frac{L_f\tan\tau_{1,L} + h_i}{L_f}\right) \tag{70}$$

Let the bow shock angle be denoted by β. If $\beta > \tau_{bowshock}$, then the shock misses the point g and the flow properties on lower surface gh are computed using the flow properties behind the oblique shock (V_2, ρ_2, a_2) as the initial conditions. Then, an expansion fan forms at point g. If $\beta \leq \tau_{bowshock}$, then either the shock is on the lip (point g) or the shock is inside the engine inlet. In either case, freestream properties are used to compute V_3, ρ_3, a_3. The following steps are used to determine the flow conditions over surface gh.

1. Calculate shock angle, β, from surface cd.

2. If $\beta > \tau_{bowshock}$, an expansion fan forms at point g and the flow properties behind the oblique shock wave are used as input to the expansion fan flow equations with a wedge angle of $\tau_{1,L}$.

3. If $\beta \leq \tau_{bowshock}$, an expansion fan forms at point g and the freestream flow properties are used as input to the expansion fan flow equations. The wedge angle in this case is only a function of angle of attack. If $\alpha = 0$, then the flow properties in region 3 are freestream, that is, $V_3 = V_\infty, \rho_3 = \rho_\infty$, and $a_3 = a_\infty$. If $\alpha > 0$, a shock forms at point g with the shock angle computed using a wedge angle of α. If $\alpha < 0$, an expansion fan forms on the underside of the engine and flow properties in region 3 are calculated using a wedge angle of $-\alpha$.

For the control surface, the flow behind the leading edge of the elevator is determined by the elevator deflection angle and the angle of attack. More specifically, if $\delta_e = -\alpha$ then both the top and bottom of the elevator experience the freestream. Therefore, $V_4 = V_5 = V_\infty$, $\rho_4 = \rho_5 = \rho_\infty$, and $a_4 = a_5 = a_\infty$. If $\delta_e > -\alpha$, then an expansion fan forms on the top of the elevator, while the bottom of the elevator experiences compression and a shock forms. In either case, the wedge angle is $\alpha + \delta_e$. If $\delta_e < -\alpha$ the a shock forms on top of elevator and an expansion fan is on the bottom of the elevator. In this case, the wedge angle for the shock and expansion fan is $-\alpha - \delta_e$.

VIII. Total Forces and Moments

Having determined the forces on each of the surfaces, the moments about the c.g. that each force produces must be determined. To do this, the location of each force on the vehicle must be computed. Figure 3 shows the forces acting on the vehicle. Consider first the upper surface with the forebody and aftbody forces given

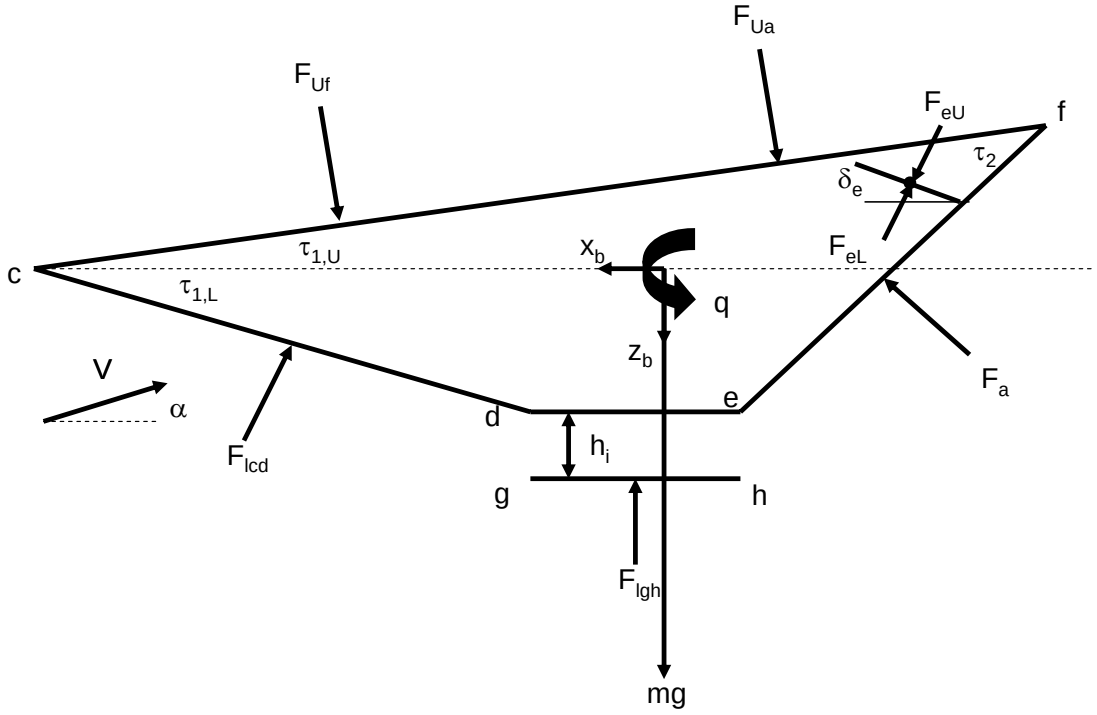

Figure 3. Forces Acting on the Hypersonic Vehicle.

in Eq. 39. The forebody force acts at the point

$$\mathbf{F}_{cf_f} : \left(\frac{\bar{x}_f}{2}, -\frac{\bar{x}_f}{2}\tan\tau_{1,U}\right) \tag{71}$$

while the upper surface afterbody force acts at

$$\mathbf{F}_{cf_a} : \left(-\frac{\bar{x}_a}{2}, -\left(\bar{x}_f + \frac{\bar{x}_a}{2}\right)\tan\tau_{1,U}\right) \tag{72}$$

For the lower surfaces,

$$\mathbf{F}_{cd} : \left(\bar{x}_f - \frac{L_f}{2}, \frac{L_f}{2}\tan\tau_{1,L}\right) \tag{73}$$

$$\mathbf{F}_{gh} : \left(\bar{x}_f - L_f - \frac{L_n}{2}, L_f\tan\tau_{1,L} + h_i\right) \tag{74}$$

The force due to the external nozzle acts at a point given by

$$\mathbf{F}_{ef} : \left(\bar{x}_f - L_f - L_n - \bar{x}_{\mathbf{F}_{ef}}\cos\left(\tau_{1,U} + \tau_2\right), L_f\tan\tau_{1,L} - \bar{x}_{\mathbf{F}_{ef}}\sin\left(\tau_{1,U} + \tau_2\right)\right) \tag{75}$$

where $\bar{x}_{\mathbf{F}_{ef}}$ is the x point of the center of mass of the pressure distribution on the rear ramp assuming an axis system centered at point e with x axis pointing along line ef and the z axis pointing up. In other words, the center of mass of the pressure distribution was computed in a local coordinate frame (local to surface ef). Then, this distance was referenced to the c.g. of the vehicle. In Eq. 75, $\bar{x}_{\mathbf{F}_{ef}}$ is given by

$$\bar{x}_{\mathbf{F}_{ef}} = \frac{L_a}{\cos\left(\tau_{1,U} + \tau_2\right)\ln\frac{P_e}{P_\infty}}\left[1 - \frac{P_\infty}{P_e - P_\infty}\ln\frac{P_e}{P_\infty}\right] \tag{76}$$

The elevator force acts at

$$\mathbf{F}_e : (-x_{cs}, -z_{cs}) \tag{77}$$

Equations 39, 40, 44, 63, and 64 give the axial and normal force components of the forces acting on the vehicle. Now, the moments due to these forces can be calculated. Positive moment is defined as clockwise or the direction that tends to increase angle of attack, while negative moment is defined as counter-clockwise. The moment arms are given by Eqs. 71 - 75, 77.

$$M_{cf_f} = -\frac{P_1\bar{x}_f^2}{2}\left(1 - \tan^2\tau_{1,U}\right) \tag{78}$$

$$M_{cf_a} = -P_1\bar{x}_a\tan^2\tau_{1,U}\left(\bar{x}_f + \frac{\bar{x}_a}{2}\right) + P_1\frac{\bar{x}_a^2}{2} \tag{79}$$

$$M_{cd} = -P_2L_f\tan\tau_{1,L}\left(\frac{L_f\tan\tau_{1,L}}{2}\right) + P_2L_f\left(\bar{x}_f - \frac{L_f}{2}\right) \tag{80}$$

$$M_{gh} = P_3L_n\left(\bar{x}_f - L_f - \frac{L_n}{2}\right) \tag{81}$$

$$M_{ef} = \pm X_{ef}\left[L_f\tan\tau_{1,L} - \bar{x}_{\mathbf{F}_{ef}}\sin\left(\tau_{1,U} + \tau_2\right)\right] - Z_{ef}\left[\bar{x}_f - L_f - L_n - \bar{x}_{\mathbf{F}_{ef}}\cos\left(\tau_{1,U} + \tau_2\right)\right] \tag{82}$$

where $\bar{x}_{\mathbf{F}_{ef}}$ is given in Eq. 76 and X_{ef}, Z_{ef} are expressed in Eq. 44. The sign on the first component of M_{ef} will depend on the vehicle's geometry. The rule used to determine the sign is as follows:

$$\begin{array}{l} +\ \ if\ \ L_f\tan\tau_{1,L} - \bar{x}_{\mathbf{F}_{ef}}\sin\left(\tau_{1,U} + \tau_2\right) > 0 \\ -\ \ if\ \ L_f\tan\tau_{1,L} - \bar{x}_{\mathbf{F}_{ef}}\sin\left(\tau_{1,U} + \tau_2\right) \leq 0 \end{array} \tag{83}$$

The moments produced by the elevator are

$$M_{e_U} = -P_5L_e\sin\delta_e z_{cs} + P_5L_e\cos\delta_e x_{cs} \tag{84}$$

$$M_{e_L} = P_4 L_e \sin\delta_e z_{cs} - P_4 L_e \cos\delta_e x_{cs} \tag{85}$$

The total aerodynamic forces and moments on the vehicle are

$$X_{total} = X_{cf_f} + X_{cf_a} + X_{cd} + X_{gh} + X_{ef} + X_{e_L} + X_{e_U} \tag{86}$$

$$Z_{total} = Z_{cf_f} + Z_{cf_a} + Z_{cd} + Z_{gh} + Z_{ef} + Z_{e_L} + Z_{e_U} \tag{87}$$

$$M_{total} = M_{cf_f} + M_{cf_a} + M_{cd} + M_{gh} + M_{ef} + M_{e_L} + M_{e_U} \tag{88}$$

IX. Stability Derivatives

The stability derivatives of interest for this vehicle configuration are $C_{Z\alpha}$, $C_{x\alpha}$, $C_{M\alpha}$, C_{Zq}, and C_{Mq}. These computations are complex and, in an attempt to simplify them, the following notation will be used when necessary:

$$\begin{aligned} L_{ef_2} &= \tfrac{(L_a-\bar{x}_a)^2}{2} - \tfrac{\bar{x}_a^2}{2} \\ L_{ef_3} &= \tfrac{(L_a-\bar{x}_a)^3}{3} + \tfrac{\bar{x}_a^3}{3} \\ L_{ef_4} &= \tfrac{(L_a-\bar{x}_a)^4}{4} - \tfrac{\bar{x}_a^4}{4} \\ L_{ef_2} &= \tfrac{(L_a-\bar{x}_a)^5}{5} + \tfrac{\bar{x}_a^5}{5} \end{aligned} \tag{89}$$

$$\begin{aligned} A_1 &= \rho_e a_e + \tfrac{(\rho_e-\rho_\infty)(a_e-a_\infty)(L_a-\bar{x}_a)^2}{L_a^2} - \tfrac{a_e}{L_a}(\rho_e-\rho_\infty)(L_a-\bar{x}_a) - \tfrac{\rho_e}{L_a}(a_e-a_\infty)(L_a-\bar{x}_a) \\ A_2 &= \tfrac{a_e}{L_a}(\rho_e-\rho_\infty) + \tfrac{\rho_e}{L_a}(a_e-a_\infty) - \tfrac{2}{L_a^2}(\rho_e-\rho_\infty)(a_e-a_\infty)(L_a-\bar{x}_a) \\ A_3 &= \tfrac{(\rho_e-\rho_\infty)(a_e-a_\infty)}{L_a^2} \end{aligned} \tag{90}$$

$$\begin{aligned} f_1 &= \tan(\tau_{1,U}+\tau_2) \\ f_2 &= L\tan\tau_{1,U} \\ f_3 &= \sin(\tau_{1,U}+\tau_2) \\ f_4 &= \cos(\tau_{1,U}+\tau_2) \end{aligned} \tag{91}$$

Additionally, the pressure on the rear ramp of the vehicle (surface ef) is given by Eq. 41, which is a function of the distance moved along the rear ramp. Thus, this pressure distribution is not constant along the surface. At point e, the pressure is given by the engine exit properties (P_e), while at point f the pressure is the freestream pressure (P_∞). An obvious choice for the temperature distribution on the rear ramp, T_{ef}, is a form like the corresponding pressure, so that

$$T_{ef}(s) \approx \frac{T_e}{1 + \frac{s}{\frac{L_a}{\cos(\tau_{1,U}+\tau_2)}}\left(\frac{T_e}{T_\infty}-1\right)} \tag{92}$$

Then, the speed of sound and density can be calculated from the definition of speed of sound and the perfect gas law:

$$\begin{aligned} a_{ef} &= \sqrt{\gamma R T_{ef}} \\ \rho_{ef} &= \tfrac{P_{ef}}{RT_{ef}} \end{aligned} \tag{93}$$

Both a_{ef} and ρ_{ef} factor into the stability derivative calculations. Unfortunately, the expressions in Eq. 93, when used in the stability derivative calculations do not allow determination of a closed-form solution. In order to facilitate a closed-form solution, the following approximations for the speed of sound and density on the rear ramp will be used in the stability derivative calculations:

$$\begin{aligned} \rho_{ef} &= \tfrac{(\rho_\infty-\rho_e)}{-L_a}(x-\{L_a-\bar{x}_a\}) + \rho_e \\ a_{ef} &= \tfrac{(a_\infty-a_e)}{-L_a}(x-\{L_a-\bar{x}_a\}) + a_e \end{aligned} \tag{94}$$

where

$$-\bar{x}_a \le x \le L_a - \bar{x_a} \tag{95}$$

These are first-order approximations, which capture the boundary conditions.

A. α Derivative of Z-Force Coefficient

To compute the change in Z-force component due to a change in angle of attack, the infinitesimal force expression that contains the vertical velocity perturbation, w, must be integrated. Thus,

$$\begin{aligned}(C_Z)_w = \frac{1}{q_\infty S}\int (d\mathbf{F})_{z-w} = \frac{1}{q_\infty S}\left[\int_{-\bar{x}_a}^{\bar{x}_f} (d\mathbf{F}_{cf})_{z-w} + \int_{\bar{x}_f-L_f}^{\bar{x}_f} (d\mathbf{F}_{cd})_{z-w}\right] \\ +\frac{1}{q_\infty S}\left[\int_{\bar{x}_f-L_f-L_n}^{\bar{x}_f-L_f} (d\mathbf{F}_{gh})_{z-w} + \int_{-\bar{x}_a}^{L_a-\bar{x}_a} (d\mathbf{F}_{ef})_{z-w}\right]\end{aligned} \tag{96}$$

where $\int (d\mathbf{F}_u)_{z-w}$ is the differential force, on the upper surface, in the z direction due to w motion. Using the appropriate differential force elements from Eq. 25 in Eq. 96 produces

$$\begin{aligned}(C_Z)_w = \frac{1}{q_\infty S}\left[\int_{-\bar{x}_a}^{\bar{x}_f} -\rho_1 a_1 w\cos\tau_{1,U}dx - \int_{\bar{x}_f-L_f}^{\bar{x}_f} \rho_2 a_2 w\cos\tau_{1,L}dx\right] \\ +\frac{1}{q_\infty S}\left[\int_{\bar{x}_f-L_f-L_n}^{\bar{x}_f-L_f} -\rho_3 a_3 w dx + \int_{\bar{x}_a}^{L_a-\bar{x}_a} -\rho_{ef} a_{ef} w\cos\left(\tau_{1,U}+\tau_2\right)dx\right]\end{aligned} \tag{97}$$

Performing the integrations yields

$$\begin{aligned}(C_Z)_w = w\frac{1}{q_\infty S}\left[-\rho_1 a_1\cos\tau_{1,U}\left(\bar{x}_f+\bar{x}_a\right) - \rho_2 a_2\cos\tau_{1,L}L_f - \rho_3 a_3 L_n\right] \\ -w\frac{\cos\left(\tau_{1,U}+\tau_2\right)}{q_\infty S}\left[A_1 L_a + A_2 L_{ef_2} + A_3 L_{ef_3}\right]\end{aligned} \tag{98}$$

If $\frac{w}{V_\infty} \ll 1$ then $\frac{w}{V_\infty} \approx \alpha$. Thus, $w = V_\infty\alpha$. Therefore,

$$\begin{aligned}\frac{\partial C_Z}{\partial\alpha} = \frac{V_\infty}{q_\infty S}\left[-\rho_1 a_1\cos\tau_{1,U}L - \rho_2 a_2\cos\tau_{1,L}L_f - \rho_3 a_3 L_n\right] \\ -\frac{V_\infty\cos\left(\tau_{1,U}+\tau_2\right)}{q_\infty S}\left[A_1 L_a + A_2 L_{ef_2} + A_3 L_{ef_3}\right]\end{aligned} \tag{99}$$

B. α Derivative of X-Force Coefficient

The change in X-force due to a change in angle of attack can be calculated using

$$\begin{aligned}(C_X)_w = \frac{1}{q_\infty S}\int (d\mathbf{F})_{x-w} = \frac{1}{q_\infty S}\left[\int_{-\bar{x}_a}^{\bar{x}_f} (d\mathbf{F}_{cf})_{x-w} + \int_{\bar{x}_f-L_f}^{\bar{x}_f} (d\mathbf{F}_{cd})_{x-w}\right] \\ +\frac{1}{q_\infty S}\left[\int_{\bar{x}_f-L_f-L_n}^{\bar{x}_f-L_f} (d\mathbf{F}_{gh})_{x-w} + \int_{-\bar{x}_a}^{L_a-\bar{x}_a} (d\mathbf{F}_{ef})_{x-w}\right]\end{aligned} \tag{100}$$

Substituting in the differential forces yields

$$\begin{aligned}(C_X)_w = \frac{1}{q_\infty S}\left[\int_{-\bar{x}_a}^{\bar{x}_f} \rho_1 a_1 w\sin\tau_{1,U}dx - \int_{\bar{x}_f-L_f}^{\bar{x}_f} \rho_2 a_2 w\sin\tau_{1,L}dx\right] \\ +\frac{1}{q_\infty S}\left[\int_{\bar{x}_f-L_f-L_n}^{\bar{x}_f-L_f} -\rho_3 a_3 w 0 dx + \int_{-\bar{x}_a}^{L_a-\bar{x}_a} \rho_{ef} a_{ef} w\sin\left(\tau_{1,U}+\tau_2\right)dx\right]\end{aligned} \tag{101}$$

Performing the integrations, simplifying, and assuming that $\frac{w}{V_\infty} \ll 1$ so that $\frac{w}{V_\infty} \approx \alpha$ gives

$$\frac{\partial C_X}{\partial\alpha} = \frac{1}{q_\infty S}V_\infty\left[\rho_1 a_1\sin\tau_{1,U}L - \rho_2 a_2\sin\tau_{1,L}L_f\right] + \frac{V_\infty\sin\left(\tau_{1,U}+\tau_2\right)}{q_\infty S}\left[A_1 L_a + A_2 L_{ef_2} + A_3 L_{ef_3}\right] \tag{102}$$

C. α Derivative of Pitching Moment Coefficient

For $C_{M\alpha}$, first find the contribution to the pitching moment due to a velocity w:

$$\begin{aligned}(C_M)_w &= \frac{1}{q_\infty S\bar{c}}\left[\int z\,(d\mathbf{F})_{x-w} - \int x\,(d\mathbf{F})_{z-w}\right] \\ &= \frac{1}{q_\infty S\bar{c}} z\left[\int_{-\bar{x}_a}^{\bar{x}_f}(d\mathbf{F}_{cf})_{x-w} + \int_{\bar{x}_f-L_f}^{\bar{x}_f}(d\mathbf{F}_{cd})_{x-w} + \int_{\bar{x}_f-L_f-L_n}^{\bar{x}_f-L_f}(d\mathbf{F}_{gh})_{x-w} + \int_{-\bar{x}_a}^{L_a-\bar{x}_a}(d\mathbf{F}_{ef})_{x-w}\right] \\ &\quad - \frac{1}{q_\infty S\bar{c}} x\left[\int_{-\bar{x}_a}^{\bar{x}_f}(d\mathbf{F}_{cf})_{z-w} + \int_{\bar{x}_f-L_f}^{\bar{x}_f}(d\mathbf{F}_{cd})_{z-w} + \int_{\bar{x}_f-L_f-L_n}^{\bar{x}_f-L_f}(d\mathbf{F}_{gh})_{z-w} + \int_{-\bar{x}_a}^{L_a-\bar{x}_a}(d\mathbf{F}_{ef})_{z-w}\right]\end{aligned} \tag{103}$$

Substituting the appropriate expressions, performing the integrations, simplifying, and assuming that $\frac{w}{V_\infty} \ll 1$ so that $\frac{w}{V_\infty} \approx \alpha$ yields

$$\begin{aligned}\frac{\partial C_M}{\partial \alpha} &= \frac{1}{q_\infty S\bar{c}}\frac{1}{2}V_\infty\left[-\rho_1 a_1 \tan\tau_{1,U}\sin\tau_{1,U}L^2 + \rho_2 a_2\tan\tau_{1,L}\sin\tau_{1,L}L_f^2\right] \\ &+\frac{V_\infty\sin(\tau_{1,U}+\tau_2)}{q_\infty S\bar{c}}\left[f_1\left(A_1L_{ef_2}+A_2L_{ef_3}+A_3L_{ef_4}\right)+\left(f_1\bar{x}_a-f_2\right)\left(A_1L_a+A_2L_{ef_2}+A_3L_{ef_3}\right)\right] \\ &+\frac{1}{q_\infty S\bar{c}}\frac{1}{2}V_\infty\left[\rho_1 a_1\cos\tau_{1,U}\left(\bar{x}_f^2-\bar{x}_a^2\right)+\rho_2 a_2\cos\tau_{1,L}L_f\left(2\bar{x}_f-L_f\right)-\rho_3 a_3 L_n\left(L_n-2\bar{x}_f+2L_f\right)\right] \\ &-\frac{V_\infty\cos(\tau_{1,U}+\tau_2)}{q_\infty S\bar{c}}\left[A_1L_{ef_2}+A_2L_{ef_3}+A_3L_{ef_4}\right]\end{aligned} \tag{104}$$

D. q Derivative of Z-Force Coefficient

The Z-force coefficient due to a pitching motion is

$$\begin{aligned}(C_Z)_q = \frac{1}{q_\infty S}\int(d\mathbf{F})_{z-q} &= \frac{1}{q_\infty S}\left[\int_{-\bar{x}_a}^{\bar{x}_f}(d\mathbf{F}_{cf})_{z-q} + \int_{\bar{x}_f-L_f}^{\bar{x}_f}(d\mathbf{F}_{cd})_{z-q}\right] \\ &+\frac{1}{q_\infty S}\left[\int_{\bar{x}_f-L_f-L_n}^{\bar{x}_f-L_f}(d\mathbf{F}_{gh})_{z-q} + \int_{-\bar{x}_a}^{L_a-\bar{x}_a}(d\mathbf{F}_{ef})_{z-q}\right]\end{aligned} \tag{105}$$

Performing the integrations and simplifying yields

$$\begin{aligned}\frac{\partial C_Z}{\partial q} &= \frac{1}{q_\infty S}\rho_1 a_1\frac{L}{2}\left[\cos\tau_{1,U}-\tan\tau_{1,U}\sin\tau_{1,U}L\right] \\ &+\frac{1}{q_\infty S}\rho_2 a_2\frac{L_f}{2}\left[\cos\tau_{1,L}\left(2\bar{x}_f-L_f\right)-\tan\tau_{1,L}\sin\tau_{1,L}L_f\right] \\ &+\frac{1}{q_\infty S}\rho_3 a_3\frac{L_n}{2}\left[-L_n+2\bar{x}_f-2L_f\right] \\ &+\frac{1}{q_\infty S}\left[\frac{L_a^2}{2}\left(f_1f_3A_1\right)-L_af_2f_3A_1+L_{ef_2}f_4A_1+\frac{\left(2L_a^3-3L_a^2\bar{x}_a\right)}{6}f_1f_3A_2-L_{ef_2}f_2f_3A_2\right] \\ &+\frac{1}{q_\infty S}\left[L_{ef_3}f_4A_2+\left(L_{ef_4}+\frac{\left(L_a-\bar{x}_a\right)^3\bar{x}_a}{3}+\frac{\bar{x}_a^4}{3}\right)f_1f_3A_3-L_{ef_3}f_2f_3A_3+L_{ef_4}f_4\right]\end{aligned} \tag{106}$$

E. q Derivative of Pitching Moment Coefficient

The pitching moment due to a pitch rate can be calculated using

$$(C_M)_q = \frac{1}{q_\infty S\bar{c}} \int z\,(d\mathbf{F})_{x-q} - \int x\,(d\mathbf{F})_{z-q}$$

$$= \frac{1}{q_\infty S\bar{c}} z \left[\int_{-\bar{x}_a}^{\bar{x}_f} (d\mathbf{F}_{cf})_{x-q} + \int_{\bar{x}_f-L_f}^{\bar{x}_f} (d\mathbf{F}_{cd})_{x-q} + \int_{\bar{x}_f-L_f-L_n}^{\bar{x}_f-L_f} (d\mathbf{F}_{gh})_{x-q} + \int_{-\bar{x}_a}^{L_a-\bar{x}_a} (d\mathbf{F}_{ef})_{x-q} \right] \tag{107}$$

$$- \frac{1}{q_\infty S\bar{c}} x \left[\int_{-\bar{x}_a}^{\bar{x}_f} (d\mathbf{F}_{cf})_{z-q} + \int_{\bar{x}_f-L_f}^{\bar{x}_f} (d\mathbf{F}_{cd})_{z-q} + \int_{\bar{x}_f-L_f-L_n}^{\bar{x}_f-L_f} (d\mathbf{F}_{gh})_{z-q} + \int_{-\bar{x}_a}^{L_a-\bar{x}_a} (d\mathbf{F}_{ef})_{z-q} \right]$$

Substituting the appropriate expressions yields, performing the integrations, and simplifying produces

$$\begin{aligned}
\frac{\partial C_M}{\partial q} = &-\frac{1}{q_\infty S\bar{c}} \rho_1 a_1 \tan^2\tau_{1,U} \left[\tan\tau_{1,U} \sin\tau_{1,U} \frac{L^3}{3} + \frac{\cos\tau_{1,U}}{6} \left(-\bar{x}_f^3 + 2\bar{x}_a^3 + 3\bar{x}_a^2 \bar{x}_f \right) \right] \\
&-\frac{1}{q_\infty S\bar{c}} \rho_2 a_2 \tan^2\tau_{1,L} \left[\tan\tau_{1,L} \sin\tau_{1,L} \frac{L_f^3}{3} - \cos\tau_{1,L} \frac{L_f}{2} \left(2\bar{x}_f - L_f \right) \right] \\
&-\frac{f_1}{q_\infty S\bar{c}} \left[\left(A_1 L_{ef_3} + A_2 L_{ef_4} + A_3 L_{ef_5} \right) \left(f_1^2 f_3 + f_1 f_4 \right) \right] \\
&-\frac{f_1}{q_\infty S\bar{c}} \left[\left(A_1 L_{ef_2} + A_2 L_{ef_3} + A_3 L_{ef_4} \right) \left(2 f_1^2 f_3 \bar{x}_a - 2 f_1 f_2 f_3 - f_2 f_4 \right) \right] \\
&-\frac{f_1}{q_\infty S\bar{c}} \left[\left(A_1 L_a + A_2 L_{ef_2} + A_3 L_{ef_3} \right) \left(f_1^2 f_3 \bar{x}_a - 2 f_1 f_2 f_3 \bar{x}_a + f_1 f_4 \bar{x}_a + f_2^2 f_3 \right) \right] \\
&-\frac{1}{q_\infty S\bar{c}} \rho_1 a_1 \left[\frac{\tan\tau_{1,U} \sin\tau_{1,U}}{6} \left(-\bar{x}_f^3 + 3\bar{x}_a^2 \bar{x}_f + 2\bar{x}_a^3 \right) + \frac{\cos\tau_{1,U}}{3} \left(\bar{x}_f^3 + \bar{x}_a^3 \right) \right] \\
&-\frac{1}{q_\infty S\bar{c}} \rho_2 a_2 \left[\frac{\tan\tau_{1,L} \sin\tau_{1,L}}{6} L_f^2 \left(2L_f - 3\bar{x}_f \right) + \cos\tau_{1,L} \frac{L_f}{3} \left(3\bar{x}_f^2 - 3\bar{x}_f L_f + L_f^2 \right) \right] \\
&-\frac{1}{q_\infty S\bar{c}} \rho_3 a_3 \left[\frac{\left(\bar{x}_f - L_f \right)^3}{3} - \frac{\left(\bar{x}_f - L_f - L_n \right)^3}{3} \right] \\
&-\frac{1}{q_\infty S\bar{c}} \left[\left(A_1 L_{ef_3} + A_2 L_{ef_4} + A_3 L_{ef_5} \right) \left(f_1 f_3 + f_4 \right) + \left(A_1 L_{ef_2} + A_2 L_{ef_3} + A_3 L_{ef_4} \right) \left(f_1 f_3 \bar{x}_a - f_2 f_3 \right) \right]
\end{aligned} \tag{108}$$

X. Engine

For hypersonic flight, the propulsion system necessary to produce the required thrust is either a rocket or a supersonic combustion ramjet (scramjet). The advantage of a scramjet over a rocket is that the scramjet is an airbreathing propulsion system, thus eliminating the need to carry the oxidizer onboard the vehicle. This, in turn, allows for increased payload. The scramjet model used in this work is identical to that used by Chavez and Schmidt.[5] Engine inlet conditions are primarily determined by the flow behind the oblique shock. The scramjet consists of 3 sections; a diffuser, a combustor, and an internal nozzle. The flow through the diffuser and nozzle is assumed to be isentropic, quasi-one-dimensional, while the flow through the combustor is assumed to be quasi-one-dimensional in a constant area duct with heat addition. The working fluid in the engine is assumed to be a perfect gas with constant specific heats. There are two control variables which affect the engine: diffuser area ratio, $\bar{A}_D$, and temperature addition in the combustor, ΔT_0. Figure 4 shows the engine model.

Inlet conditions to the diffuser, which are inlet conditions to the engine module, are determined from the flow analysis of the vehicle's lower forebody and vehicle geometry. The lower forebody flow is turned parallel to surface cd. To determine the engine inlet conditions, the flow must be turned parallel to the engine, with the turning angle given by $\tau_{1,L}$. Oblique shock relations are used to determine the engine inlet flow

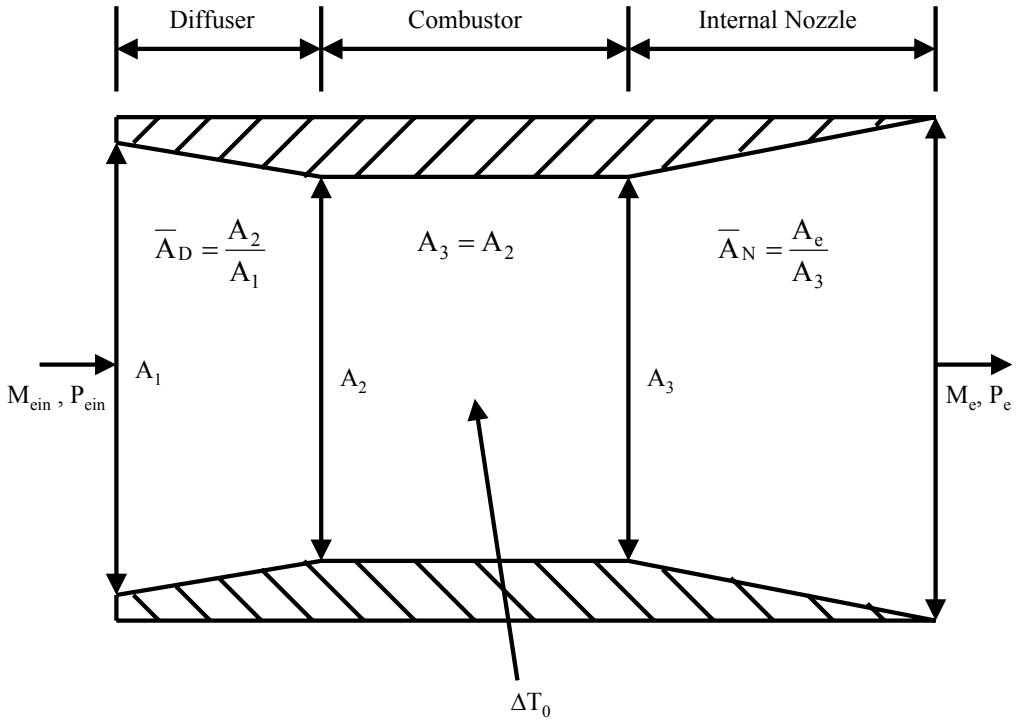

Figure 4. Scramjet Engine.

properties, with the flow properties in region 2 being the input, and $M_{e_{in}}, P_{e_{in}}$, and $T_{e_{in}}$ being the outputs of the flow calculations. The engine inlet Mach number, pressure, and temperature are $M_{e_{in}}, P_{e_{in}}$, and $T_{e_{in}}$, respectively. By turning the flow to be parallel to the engine, a force and hence moment is imparted on the vehicle. The force is given by

$$\begin{aligned} F_{x_{inlet}} &= \gamma M_2^2 P_2 \left(1 - \cos\left(\tau_{1,L} + \alpha\right)\right) \frac{\frac{A_e}{b}}{A_d A_n} \\ F_{z_{inlet}} &= \gamma M_2^2 P_2 \sin\left(\tau_{1,L} + \alpha\right) \frac{\frac{A_e}{b}}{A_d A_n} \end{aligned} \tag{109}$$

This force acts at point d in Figure 1. Hence, the force acts at

$$\mathbf{r}_{inlet} = \begin{bmatrix} \bar{x}_f - L_f & L_f \tan\tau_{1,L} \end{bmatrix} \tag{110}$$

Thus, the moment produced is given by

$$M_{inlet} = L_f \tan\tau_{1,L} F_{x_{inlet}} - \left(\bar{x}_f - L_f\right) F_{z_{inlet}} \tag{111}$$

Now, the flow must be propagated through each section of the scramjet to determine the engine output properties. For the diffuser, continuity is applied to determine the Mach number at the diffuser exit/combustor inlet:

$$\frac{\left[1 + \frac{1}{2}\left(\gamma - 1\right) M_c^2\right]^{\left(\frac{\gamma+1}{\gamma-1}\right)}}{M_c^2} = \bar{A}_D^2 \frac{\left[1 + \frac{1}{2}\left(\gamma - 1\right) M_{e_{in}}^2\right]^{\left(\frac{\gamma+1}{\gamma-1}\right)}}{M_{e_{in}}^2} \tag{112}$$

where M_c is the Mach number at the combustor inlet and $M_{e_{in}}$ is the Mach number at the engine inlet. The pressures and temperatures at the combustor inlet are given by

$$P_c = P_{e_{in}} \left[\frac{1 + \frac{1}{2}\left(\gamma - 1\right) M_{e_{in}}^2}{1 + \frac{1}{2}\left(\gamma - 1\right) M_c^2}\right]^{\frac{\gamma}{\gamma-1}} \tag{113}$$

$$T_c = T_{e_{in}} \left[\frac{1 + \frac{1}{2}\left(\gamma - 1\right) M_{e_{in}}^2}{1 + \frac{1}{2}\left(\gamma - 1\right) M_c^2}\right] \tag{114}$$

where P_c and T_c are the pressure and temperature at the combustor inlet, and $P_{e_{in}}$ and $T_{e_{in}}$ are the pressure and temperature at the engine inlet. For the combustor, the exit Mach number, temperature, and pressure are calculated using

$$\frac{M_n^3\left[1 + \frac{1}{2}\left(\gamma - 1\right) M_n^2\right]}{\left(\gamma M_n^2 + 1\right)^2} = \frac{M_c^3\left[1 + \frac{1}{2}\left(\gamma - 1\right) M_c^2\right]}{\left(\gamma M_c^2 + 1\right)^2} + \frac{M_c^2}{\left(\gamma M_c^2 + 1\right)^2} \frac{T_0}{T_c} \tag{115}$$

$$P_n = P_c \frac{\gamma M_c^2 + 1}{\gamma M_n^2 + 1} \tag{116}$$

$$T_n = T_c \left(\frac{\gamma M_c^2 + 1}{\gamma M_n^2 + 1} \frac{M_n}{M_c}\right)^2 \tag{117}$$

where M_n, P_n, and T_n are the Mach number, pressure, and temperature at the inlet to the nozzle, respectively and T_0 is the increase in total temperature across the combustor due to the combustion of fuel. For the nozzle, the exit properties are

$$\frac{\left[1 + \frac{1}{2}\left(\gamma - 1\right) M_e^2\right]^{\left(\frac{\gamma+1}{\gamma-1}\right)}}{M_e^2} = \bar{A}_N^2 \frac{\left[1 + \frac{1}{2}\left(\gamma - 1\right) M_n^2\right]^{\left(\frac{\gamma+1}{\gamma-1}\right)}}{M_n^2} \tag{118}$$

where M_c is the Mach number at the combustor inlet and M_2 is the Mach number in region 2 (engine inlet). The pressures and temperatures at the combustor inlet are given by

$$P_e = P_n \left[\frac{1 + \frac{1}{2}\left(\gamma - 1\right) M_n^2}{1 + \frac{1}{2}\left(\gamma - 1\right) M_e^2}\right]^{\frac{\gamma}{\gamma-1}} \tag{119}$$

$$T_e = T_n \left[\frac{1 + \frac{1}{2}(\gamma - 1) M_n^2}{1 + \frac{1}{2}(\gamma - 1) M_e^2} \right] \tag{120}$$

where M_e, P_e, and T_e are the Mach number, pressure, and temperature at the engine exit, respectively, and $\bar{A}_N$ is the internal nozzle ratio defined as the ratio of the nozzle exit area to the nozzle inlet area.

The thrust per unit width of the engine module is given by[4]

$$T = \dot{m}_o (V_e - V_\infty) + (p_e - p_\infty) \frac{A_e}{b} - (p_2 - p_\infty) \frac{\frac{A_e}{b}}{A_D A_N} \tag{121}$$

where T is the engine thrust, $\dot{m}_o$ is the mass flow through the engine, V_e, p_e are the flow velocity and pressure at the engine exit, V_2, p_2 are the flow velocity and pressure at the engine inlet, p_∞ is the freestream pressure, A_e/b is the exit area per unit width, A_D is the diffuser area ratio, and A_N is the nozzle area ratio. The moment produced by the thrust force is

$$M_{engine} = \left(L_f \tan \tau_{1,L} + \frac{h_i}{2} \right) T \tag{122}$$

The mass flow through the engine is a function of the shock angle. Essentially, in order to calculate $\dot{m}_o$, it is necessary to calculate how much mass flow the engine captures. Figure 5 sets up the geometry for this calculation. It is assumed that the vehicle is operating such that the lower forebody surface see either

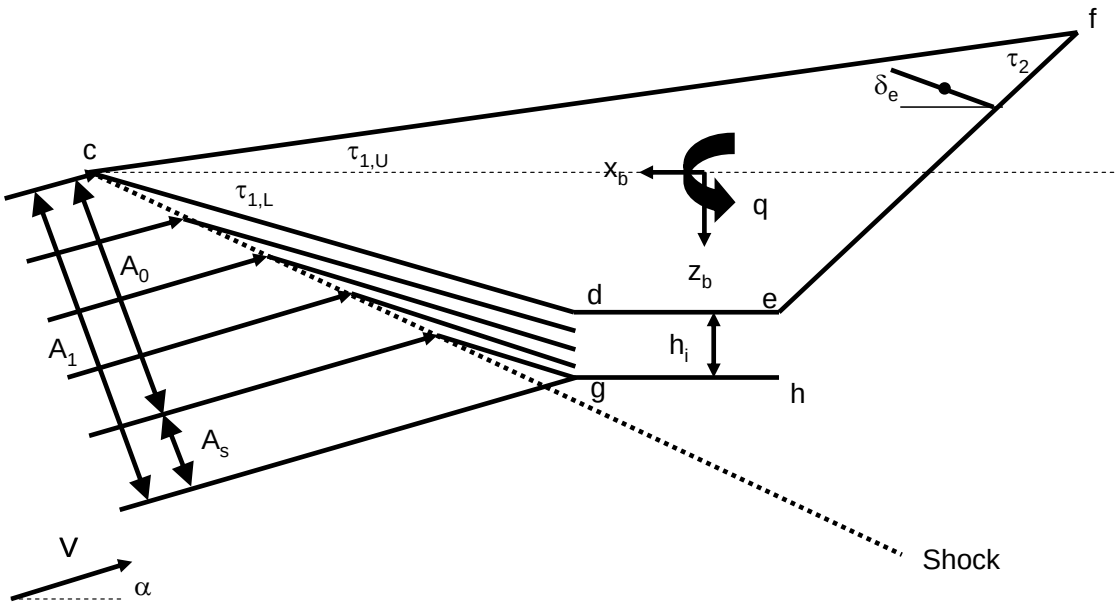

Figure 5. Geometry for Mass Flow Capture Area.

the freestream ($\alpha = -\tau_{1,L}$) or a shock forms off the forebody surface. Let the engine inlet capture area be denoted by A_0 and the spill area be denoted by A_s. Then, if freestream conditions occur, $A_0 = h_i$. When a shock forms, use Figure 5 to compute the capture area, which becomes

$$\begin{aligned} A_0 &= \frac{(L_f - 2\{L_f - (L_f \tan \tau_{1,L} + h_i) \cot(\beta_{lcd} - \alpha)\})}{\cos(\beta_{lcd} - \alpha)} \sin \beta_{lcd} \\ A_1 &= \frac{(L_f \tan \tau_{1,L} + h_i)}{\sin \theta_1} \sin(\alpha + \theta_1) \end{aligned} \tag{123}$$

where β_{lcd} is the shock angle for lower surface cd and θ_1 is defined as

$$\theta_1 = \tan^{-1} \left(\frac{L_f \tan \tau_{1,L} + h_i}{L_f} \right) \tag{124}$$

The mass flow through the engine becomes

$$\dot{m}_o = p_\infty M_\infty \sqrt{\frac{\gamma}{RT_\infty}} A_0 \tag{125}$$

With the inclusion of the stability derivatives, the engine inlet turning force and moment, and the thrust and resulting moment, the total aerodynamic forces and moments on the vehicle are

$$X_{total} = X_{cf_f} + X_{cf_a} + X_{cd} + X_{gh} + X_{ef} + X_{e_L} + X_{e_U} + q_\infty S \frac{\partial C_X}{\partial \alpha}\alpha + F_{x_{inlet}} + T \tag{126}$$

$$Z_{total} = Z_{cf_f} + Z_{cf_a} + Z_{cd} + Z_{gh} + Z_{ef} + Z_{e_L} + Z_{e_U} + q_\infty S \frac{\partial C_Z}{\partial \alpha}\alpha + + q_\infty S \frac{\partial C_Z}{\partial q}\frac{q\bar{c}}{2V_\infty} + F_{z_{inlet}} \tag{127}$$

$$M_{total} = M_{cf_f} + M_{cf_a} + M_{cd} + M_{gh} + M_{ef} + M_{e_L} + M_{e_U} + q_\infty S\bar{c} \frac{\partial C_M}{\partial \alpha}\alpha + q_\infty S\bar{c} \frac{\partial C_M}{\partial q}\frac{q\bar{c}}{2V_\infty} + M_{inlet} + M_{engine} \tag{128}$$

XI. Results

At this point, only initial simulation results are available. Currently, the model has been simulated open-loop, with a fixed control surface deflection, to ensure that the model is operating correctly. One point of interest that can be obtained from this simple simulation is the contribution to the forces and moments due to the inclusion of unsteady effects. Figure 6 shows the steady and unsteady X force, Figure 7 shows the steady and unsteady Z force, and Figure 8 shows the steady and unsteady pitching moment. Obviously, the unsteady components will have an impact on the total forces and moments, as these terms are not negligible compared to the steady terms.

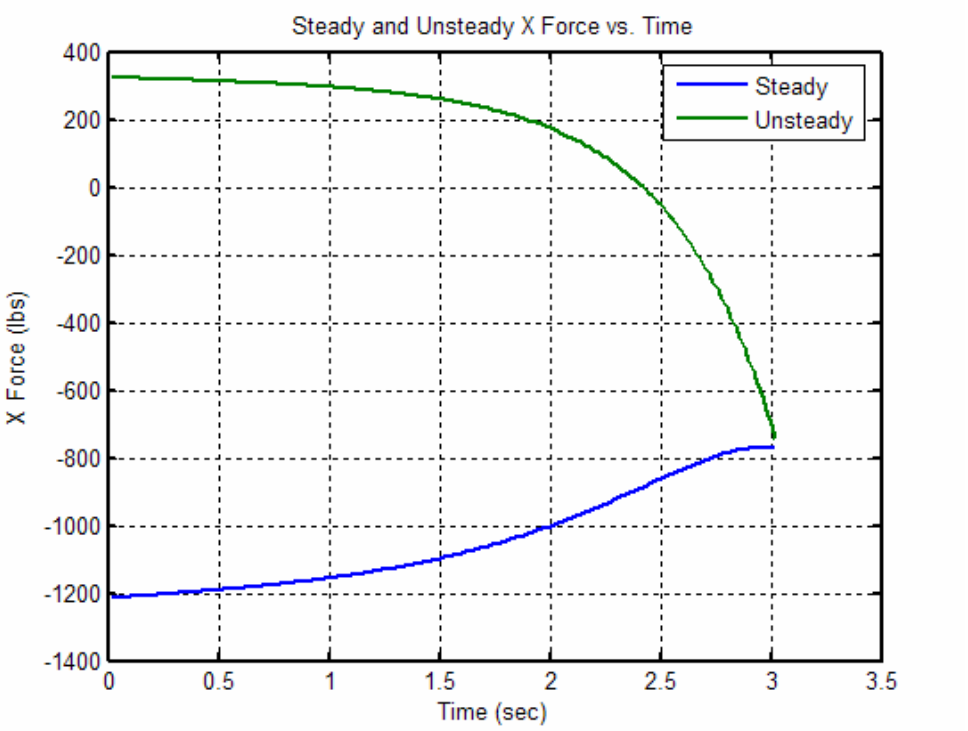

Figure 6. Steady and Unsteady X Forces.

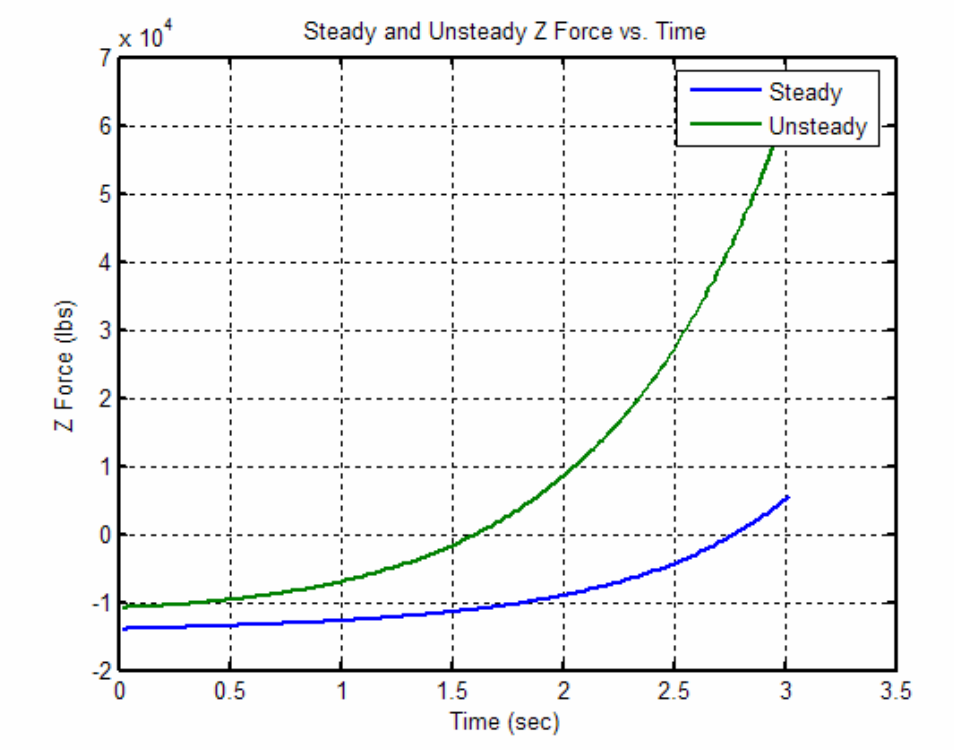

Figure 7. Steady and Unsteady Z Forces.

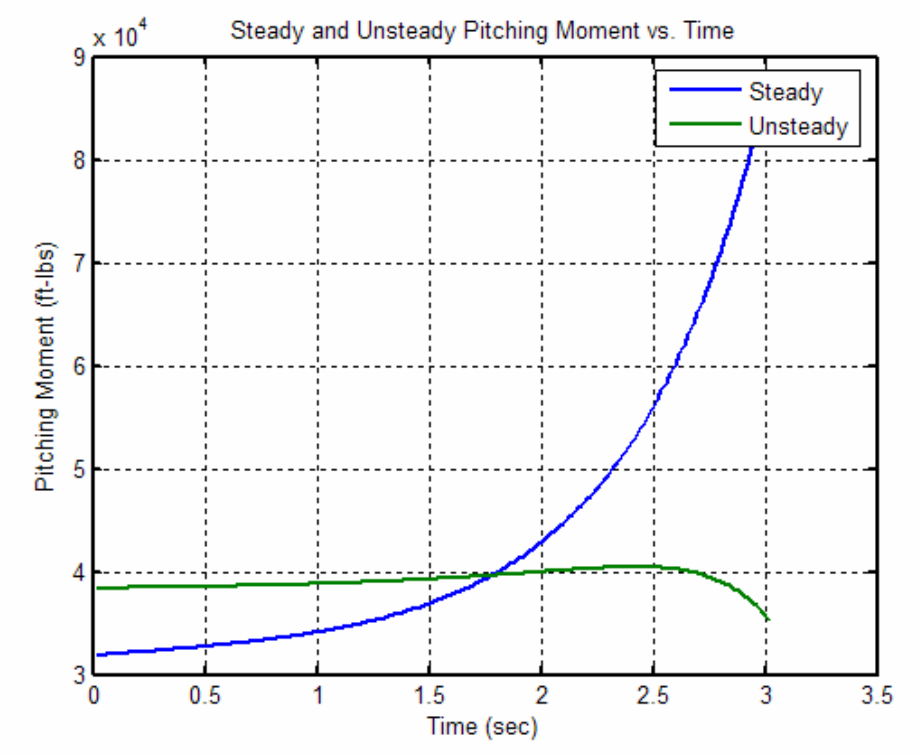

Figure 8. Steady and Unsteady Pitching Moments.

XII. Conclusions

In this work, piston theory is used to develop a model for the longitudinal dynamics of a hypersonic vehicle. In particular, velocities of flow normal to the surface of the vehicle are used in a first order piston theory framework to determine the pressures on the surfaces of the vehicle. The pressures are then integrated over the body to determine the forces acting on the vehicle. Piston theory is useful here because it allows the inclusion of the unsteady aerodynamic effects, which are not captured using other techniques.

References

[1]Lighthill, M., "Oscillating Airfoils at High Mach Number," *Journal of the Aeronautical Sciences*, Vol. 20, No. 6, 1953, pp. 402–406.

[2]Ashley, H. and Zartarian, G., "Piston Theory - A New Aerodynamic Tool for the Aeroelastician," *Journal of the Aeronautical Sciences*, 1956, pp. 1109–1118.

[3]Tarpley, C. and Lewis, M., "Stability Derivatives for a Hypersonic Caret-Wing Waverider," *Journal of Aircraft*, Vol. 32, No. 4, 1995, pp. 795–803.

[4]Bolender, M. A. and Doman, D. B., "A Non-Linear Model for the Longitudinal Dynamics of a Hypersonic Airbreathing Vehicle," *Proceedings of the 2005 Guidance, Navigation and Control Conference*, AIAA Paper No. 2005-6255, August 2005.

[5]Chavez, F. and Schmidt, D., "Analytical Aeropropulsive/Aeroelastic Hypersonic-Vehicle Model with Dynamic Analysis," *Journal of Guidance, Control, and Dynamics*, Vol. 17, No. 6, 1994, pp. 1308–1319.